https://doi.org/10.5194/egusphere-2026-3985
Preprint. Discussion started: 24 July 2026

A global assessment of warm-phase convective invigoration from aerosol-cloud interactions. Part 1: Theory

Casey J. Wall[1,2]

[1]Department of Meteorology, Stockholm University, Stockholm, 106 91, Sweden
[2]Bolin Centre for Climate Research, Stockholm University, Stockholm, 106 91, Sweden

Correspondence to: Casey J. Wall (casey.wall@misu.su.se)

Abstract. The theory of warm-phase convective invigoration from aerosol-cloud interactions posits that polluted cloud updrafts consume supersaturation more readily, causing them to release latent heat sooner and attain larger buoyancies and updraft speeds. An analytical model is developed to predict how much this mechanism changes cloud-updraft speeds when the cloud-droplet number concentration increases but the meteorological environment is fixed. For any perturbation in cloud-droplet number concentration, the model predicts an optimal updraft speed for warm-phase invigoration. Updrafts that are much slower than the optimal value experience invigoration that is directly proportional to the non-polluted updraft speed. In contrast, updrafts that are much faster than the optimal value experience a powerful feedback mechanism that resists invigoration due to changes in the drag force. For typical atmospheric conditions, shallow convective updrafts are generally closer to the optimal updraft speed than deep convective updrafts, making shallow convective clouds more susceptible to warm-phase invigoration. These predictions constrain the conditions under which substantial warm-phase invigoration can be expected to occur in nature.

1 Introduction

Aerosol-cloud interactions are one of the largest sources of uncertainty in the scientific understanding of the human influence on climate. Anthropogenic aerosols are known to enhance lightning flash rates and initiate or suppress precipitation in different environments, and they constitute the greatest source of uncertainty in the historical radiative forcing of climate (Thornton et al., 2017; Toll et al., 2024; Bellouin et al., 2020). Developing a theoretical foundation to explain aerosol-cloud interactions is a major research goal.

One class of aerosol-cloud interaction mechanisms is known as convective invigoration. According to this idea, a larger number concentration of cloud condensation nuclei perturbs cloud microphysics in ways that cause convective cloud parcels to rise faster. At least three theories have been proposed, and all of them begin with the fact that a larger concentration of cloud condensation nuclei causes convective clouds to form smaller but more numerous droplets at the cloud base. One theory argues that the increase in cloud-droplet number concentration reduces precipitation formed by droplet collision and coalescence in liquid clouds, causing more cloud water to be lost through evaporation instead of

https://doi.org/10.5194/egusphere-2026-3985
Preprint. Discussion started: 24 July 2026

precipitation. This moistens the free troposphere and encourages the development of deep convection (Abbott and Cronin, 2021; Chua and Ming, 2020). Another theory argues that the suppression of precipitation via droplet collision and coalescence causes deep convective updrafts to lift more liquid condensate above the freezing level. This changes the updraft buoyancy aloft by modifying hydrometeor loading and latent-heat release from droplet freezing (Rosenfeld et al., 2008; Igel and van den Heever, 2021). A third theory argues that the larger cloud-droplet number concentrations found in polluted clouds cause the updrafts to consume supersaturation more readily. Polluted cloud updrafts thus release latent heat sooner, attain greater buoyancies, and rise faster. The third theory, called warm-phase convective invigoration, is the focus of this study.

The theory of warm-phase convective invigoration has been heavily debated. Perhaps the most striking evidence in support of the theory was presented by Fan et al. (2018). They reported a correlation between boundary layer aerosol number concentration and deep convective updraft speed in observations over the Amazon, and they attributed this correlation to warm-phase convective invigoration using cloud-resolving-model simulations. However, the observed correlation was later shown to be insignificant when different methodologies were used, and the cloud-resolving model was shown to have a microphysical bias that causes warm-phase invigoration to be unrealistically strong (Öktem et al., 2023; Romps et al., 2023). Although the evidence in favor of warm-phase invigoration is contested, the mechanism might still operate in nature. A stronger theoretical basis and observational constraints on convective cloud properties are needed to determine the magnitude of warm-phase invigoration more definitively (Varble et al., 2023; Fan et al., 2025).

The purpose of this paper is to develop an analytical model that predicts warm-phase convective invigoration from perturbations in the cloud-droplet number concentration. The model is similar to a theory developed by Romps et al. (2023), except that warm-cloud microphysics are added to the governing equations and time-dependent solutions and feedback analysis are presented to interpret the results. This framework is applied to derive necessary conditions for substantial warm-phase convective invigoration. In a companion paper, some of the model parameters are estimated with aircraft observations to infer warm-phase invigoration in a variety of environments (Wall et al., 2026). Taken together, this work assesses cloud susceptibility to warm-phase convective invigoration in a range of environments across the globe.

2 Physical Model

Consider a thermal rising in a convective cloud. The thermal contains liquid droplets but no ice crystals, and it has cloud-droplet number concentration n, vertical wind speed w, temperature T, and supersaturation S (equal to the relative humidity minus one). The thermal occurs in relatively clean conditions with low aerosol concentrations. Next consider a second thermal in a different cloud that is exposed to more aerosol pollution. Variables that correspond to the polluted and clean thermals are denoted with and without a hat, respectively. The two thermals have the same size, fractional entrainment rate, liquid-water content, and meteorological environment, but the polluted thermal has a larger cloud-droplet number concentration, causing it to consume supersaturation more readily. This, in turn, causes the polluted thermal to have

https://doi.org/10.5194/egusphere-2026-3985
Preprint. Discussion started: 24 July 2026

supersaturation $\hat{S}$, temperature $\hat{T}$, and updraft speed $\hat{w}$ that differ from their counterparts in the clean thermal. Because the macroscopic cloud properties, liquid-water content, and environmental conditions are held constant, warm-phase convective invigoration is the sole cause of the difference in updraft speed between the two thermals. Thus, $\Delta w = \hat{w} - w$ represents warm-phase invigoration resulting from the difference in cloud-droplet number concentrations between clean and polluted conditions with the meteorological environment held fixed. The main goal of this work is to derive an expression for this quantity.

The first governing principle of the model is energy conservation. Let $h \equiv gz + c_p T + L(1+S)q^*(T)$ be the moist static energy in the clean thermal, where g is the gravitational acceleration, z is height, c_p is the specific heat capacity of air at constant pressure, L is the latent enthalpy of evaporation, and $q^*(T)$ is the saturation specific humidity. Similarly, let $\hat{h} \equiv gz + c_p\hat{T} + L(1+\hat{S})q^*(\hat{T})$ be the moist static energy of the polluted thermal. The moist static energy changes with height according to $\frac{dh}{dz} = -\epsilon(h_e - h)$ and $\frac{d\hat{h}}{dz} = -\epsilon(h_e - \hat{h})$, where ϵ is the fractional entrainment rate and h_e is the moist static energy of the environment at the same height. The cloud-base moist static energy, ϵ, and h_e are assumed to be the same for the two thermals. Thus, $h(z) = \hat{h}(z)$ for any height within the cloud. It follows from the definition of moist static energy that

$$c_p T + L(1+S)q^*(T) = c_p\hat{T} + L\left(1+\hat{S}\right)q^*\left(\hat{T}\right). \tag{1}$$

This equation states that perturbations in the cloud-droplet number concentration do not affect the overall moist static energy in the thermals, but they do affect how the moist static energy is partitioned between sensible and latent heat.

The saturation specific humidity in the two thermals are related to one another via the Clausius-Clapeyron relation:

$$q^*\left(\hat{T}\right) \approx q^*(T) + \frac{Lq^*(T)}{R_v T^2}\left(\hat{T} - T\right), \tag{2}$$

where R_v is the specific gas constant for water vapor. Substituting this relation into Eq. 1 leads to

$$-c_p\left(\hat{T} - T\right) = Lq^*(T)\left[\left(1+\hat{S}\right)\left(1 + \frac{L}{R_v T^2}\left(\hat{T} - T\right)\right) - (1+S)\right] \approx Lq^*(T)\left[\hat{S} - S + \frac{L}{R_v T^2}\left(\hat{T} - T\right)\right]. \tag{3}$$

In the final step, I have used the fact that $\hat{S}$ and $\frac{L}{R_v T^2}\left(\hat{T} - T\right)$ are typically at least one order of magnitude smaller than one. This equation can be rearranged to solve for the temperature difference between the two thermals:

$$\hat{T} - T = -\frac{Lq^*(T)}{c_p + \frac{L^2 q^*(T)}{R_v T^2}}\left(\hat{S} - S\right). \tag{4}$$

The second governing principle of the model is the conservation of vertical momentum. The clean thermal is assumed to rise at its steady-state terminal ascent rate, in which the drag force acting on the thermal, F_d, balances the buoyancy of the thermal, b. The assumption of a force balance is supported by estimates of the momentum budget of

https://doi.org/10.5194/egusphere-2026-3985
Preprint. Discussion started: 24 July 2026

thermals tracked in numerical simulations and observations (Romps and Charn, 2015; Romps and Öktem, 2015). The vertical momentum equation is thus given by:

$$0 = F_d + b. \tag{5}$$

The thermals are assumed to have a spherical shape with radius r. Drag is expressed as

$$F_d = -\frac{3c_d}{8r} w^2, \tag{6}$$

where c_d is an effective drag coefficient. Buoyancy is approximated by

$$b \approx g\frac{T-T_e}{T_e} \approx g\frac{T-T_e}{T}, \tag{7}$$

where T_e is the environmental temperature. Eq. 5-7 apply to the clean thermal, and an analogous set of equations apply to the polluted thermal. By subtracting the vertical momentum equation of one thermal from that of the other and substituting the relations for drag and buoyancy, it can be shown that

$$g\frac{T-\hat{T}}{T} \approx \frac{3c_d}{8r}(w^2 - \widehat{w}^2). \tag{8}$$

Finally, substituting Eq. 4 into Eq. 8 leads to a relation between the updraft speed and supersaturation of the two thermals:

$$\widehat{w}^2 = w^2 + \frac{ra}{c_d}(S - \hat{S}), \tag{9}$$

where

$$a \equiv \frac{8}{3}\frac{gLq^*(T)}{c_pT + \frac{L^2q^*(T)}{R_vT}}. \tag{10}$$

Eq. 1-10 were first derived by Romps et al. (2023).

The third component of the model represents warm-cloud microphysics. The supersaturation in the clean thermal evolves according to

$$\frac{dS}{dt} = Q_1 - Q_2,$$

where Q_1 is the source of supersaturation due to cooling from adiabatic expansion and Q_2 is the sink of supersaturation due to condensation. I assume that $|Q_1| \approx |Q_2|$ and that $|Q_1|$ and $|Q_2|$ are much larger than $|\frac{dS}{dt}|$. Under these conditions, S can be approximated by the quasi-steady supersaturation, given by

$$S \approx F\frac{w}{n\bar{D}}, \tag{11}$$

where F is a function of temperature and pressure and $\bar{D}$ is the mean cloud-droplet diameter. This approximation is justified on theoretical grounds and has been validated in convection-permitting-model simulations (Korolev and Mazin, 2003; Romps et al., 2023). A similar relation holds for the polluted thermal. The supersaturation difference between the two thermals is

$$S - \hat{S} = S\left(1 - \frac{\hat{S}}{S}\right) \approx S\left(1 - \frac{\widehat{w}}{w}\frac{n\bar{D}}{\hat{n}\hat{\bar{D}}}\right). \tag{12}$$

In the final step, I have ignored the small difference in F between the two thermals because F is a weak function of temperature and pressure (Romps, 2025).

https://doi.org/10.5194/egusphere-2026-3985
Preprint. Discussion started: 24 July 2026

Finally, a relationship between the liquid water content (LWC) in the two thermals must be assumed. LWC in the clean thermal is given by

$$LWC = \frac{4}{3}\pi\left(\gamma\frac{\bar{D}}{2}\right)^{3} n\rho_l,$$

where γ is the volume-weighted mean droplet diameter divided by $\bar{D}$ and ρ_l is the density of liquid water. A similar equation holds for the polluted thermal. Assuming that LWC and γ are the same for the two thermals, it follows that

$$\frac{\bar{D}}{\bar{\hat{D}}} = \left(\frac{n}{\hat{n}}\right)^{-1/3}. \tag{13}$$

By making this assumption, I am ignoring potential changes in the autoconversion and entrainment rates that are caused by changes in the cloud-droplet size distribution.

Combining Eq. 9, 12, and 13 and rearranging leads to a quadratic polynomial in $\hat{w}$:

$$\hat{w}^2 + \hat{w}\left(\frac{ra}{c_d}\frac{S}{w}\left(\frac{\hat{n}}{n}\right)^{-\frac{2}{3}}\right) + \left(-w^2 - \frac{ra}{c_d}S\right) = 0.$$

Selecting the positive root and subtracting w leads to the following relation for warm-phase convective invigoration:

$$\Delta w = \hat{w} - w = -\frac{ra}{2c_d}\frac{S}{w}\left(\frac{\hat{n}}{n}\right)^{-\frac{2}{3}} - w + \sqrt{\left(\frac{ra}{2c_d}\frac{S}{w}\left(\frac{\hat{n}}{n}\right)^{-\frac{2}{3}}\right)^{2} + w^2 + \frac{ra}{c_d}S}\,. \tag{14}$$

3 Results

3.1 General Characteristics of Solutions

The solutions for Δw depend on r, c_d, a, S, w, and $\hat{n}/n$. As a first step, typical values are selected for the parameters to reduce the dimensions of the solution space. Observations and numerical simulations of cumulus clouds indicate that r typically varies between 200 m and 1000 m and c_d typically varies between 0.2 and 1 (Romps and Charn, 2015; Romps and Öktem, 2015; Hernandez-Deckers and Sherwood, 2016; Morrison and Peters, 2018). a is a function of temperature and pressure that typically varies between 0.8 and 1.1 m s^{-2} (Romps et al., 2023). Unless otherwise stated, these parameters will be fixed to values that are close to the midpoints of their typical ranges, including $r = 600$ m, $c_d = 0.6$, and $a = 1$ m s^{-2}. S is often between 0.1% and 1%, but $S \approx 10\%$ has been reported in some deep convective situations (Prabha et al., 2011; Fan et al., 2018). To span all of these possibilities, S is set to 0.1%, 1%, and 10%. Finally, $\hat{n}/n$ is set to 2, 5, and 10 to represent typical variations in the cloud-droplet number concentration that arise from anomalies in cloud-condensation-nuclei concentrations (Boucher and Lohmann, 1995).

Warm-phase invigoration is presented as a function of S, w, and $\hat{n}/n$ in Fig. 1. For a given value of S, Δw increases with $\hat{n}/n$. This reflects the fact that a larger perturbation in cloud-droplet number concentration causes stronger invigoration of cloud updrafts. For a given value of $\hat{n}/n$, Δw also increases with S. This reflects the fact that updrafts with larger supersaturation experience larger absolute changes in buoyancy when the cloud-droplet number concentration is perturbed.

https://doi.org/10.5194/egusphere-2026-3985
Preprint. Discussion started: 24 July 2026

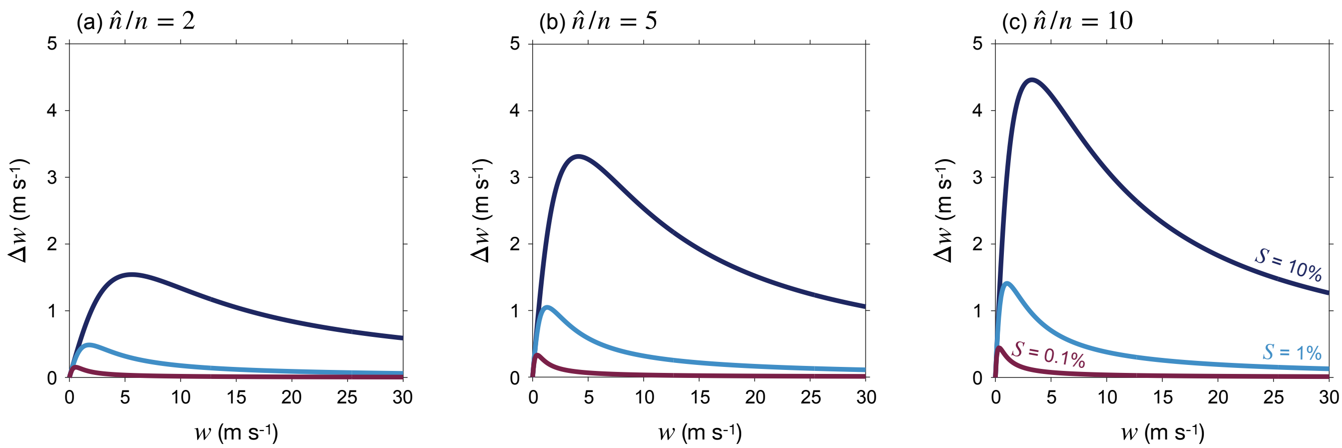

Figure 1: Warm-phase convective invigoration from aerosol-cloud interactions (Δw) plotted as a function of the updraft speed in the clean thermal (w). The ratio of cloud-droplet number concentrations between the polluted and clean thermals ($\hat{n}/n$) is varied between (a) 2, (b) 5, and (c) 10. In each panel, the supersaturation of the clean thermal (S) is varied between 0.1%, 1%, and 10%.

All of the solutions for Δw have a single peak, indicating the existence of an optimal updraft speed for warm-phase invigoration (Fig. 1). To explain this trait, I note that a characteristic updraft scale given by $\tilde{w} \equiv \left(\frac{raS}{c_d}\right)^{1/2}$ naturally emerges in the expression for Δw (Eq. 14). In physical terms, $\tilde{w}$ represents the updraft speed that would occur if an air parcel starts from rest with supersaturation S, condenses water vapor until $S = 0\%$, and then rises at its new terminal velocity. Typical values include $\tilde{w} \approx 1$ m s^{-1} when $S = 0.1\%$, $\tilde{w} \approx 3$ m s^{-1} when $S = 1\%$, and $\tilde{w} \approx 10$ m s^{-1} when $S = 10\%$ (Fig. 2). By applying the definition of $\tilde{w}$ to Eq. 14, the expression for Δw can be simplified to a non-dimensional form:

$$\Delta W = -\frac{\beta}{2W} - W + \sqrt{\left(\frac{\beta}{2W}\right)^2 + W^2 + 1}\,, \tag{15}$$

where $W \equiv \frac{w}{\tilde{w}}$ and $\beta \equiv \left(\frac{\hat{n}}{n}\right)^{-2/3}$. Any solution for Δw can be reconstructed by scaling ΔW by the appropriate value of $\tilde{w}$.

https://doi.org/10.5194/egusphere-2026-3985
Preprint. Discussion started: 24 July 2026

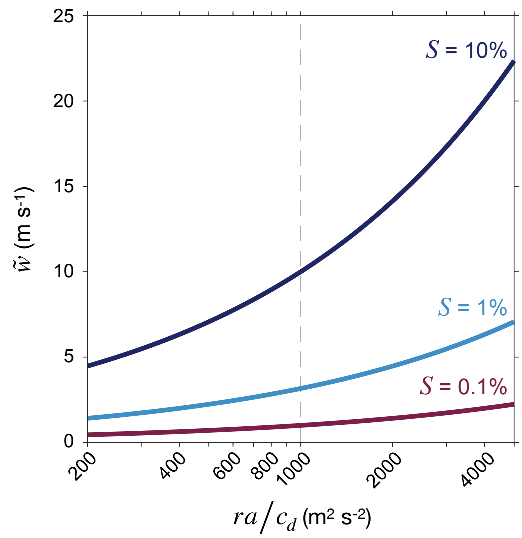

Figure 2: Characteristic updraft scale ($\tilde{w}$) plotted as a function of ra/c_d with S set to 0.1%, 1%, and 10%. The dashed line shows the default value of ra/c_d that is used throughout the study unless stated otherwise.

The limiting behavior of the solutions can be obtained from the non-dimensional equation. If $W \gg \left(\frac{\beta}{2}\right)^{1/2}$ or $W \ll \left(\frac{\beta}{2}\right)^{1/2}$, then Eq. 15 can be approximated with a first-order Taylor series in W^{-1} or W, respectively. The approximate solutions are

$$\Delta W \approx \begin{cases} W(\beta^{-1} - 1), & W \ll \left(\frac{\beta}{2}\right)^{1/2} \\ \frac{1-\beta}{2W}, & W \gg \left(\frac{\beta}{2}\right)^{1/2} \end{cases}. \tag{16}$$

ΔW vanishes in the limit as $W \to 0$ and $W \to \infty$ (Fig. 3). This implies that updrafts that rise much faster or slower than $\tilde{w}$ experience negligible warm-phase invigoration. The optimal updraft speed for warm-phase invigoration has the same order of magnitude as $\tilde{w}$.

https://doi.org/10.5194/egusphere-2026-3985
Preprint. Discussion started: 24 July 2026

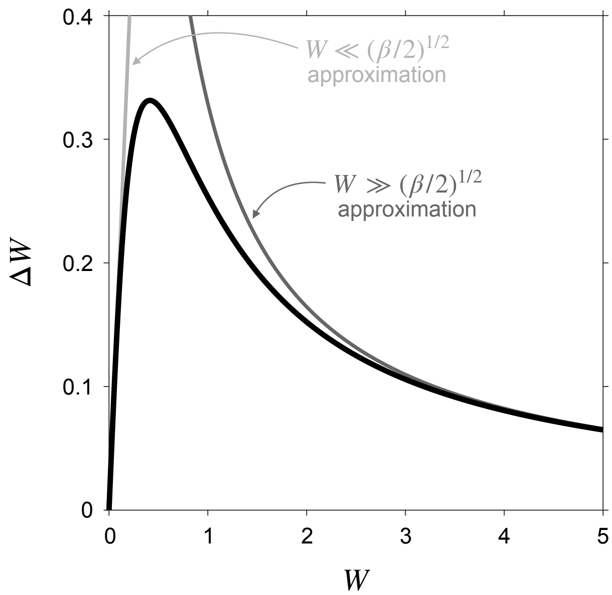

Figure 3: Warm-phase convective invigoration plotted as a function of the updraft speed in the clean thermal in non-dimensional form ($W = w/\tilde{w}$). Thin grey lines show the approximate solutions for $W \ll \left(\frac{\beta}{2}\right)^{1/2}$ and $W \gg \left(\frac{\beta}{2}\right)^{1/2}$. A value of $\frac{\hat{n}}{n} = 5$ is used.

3.2 Time-Dependent Solutions

The contrast in warm-phase invigoration for fast and slow updrafts can be further explored by temporarily relaxing the assumption of steady-state updraft speeds and predicting how ΔW evolves in time. Here, I assume that the clean thermal rises at its steady-state terminal velocity throughout its entire ascent of the cloud, but the polluted thermal does not. Instead, the polluted thermal starts with the same updraft speed as the clean thermal at time $t = 0$ s and then adjusts toward its own terminal velocity. The polluted thermal initially experiences the same drag force as the clean thermal, but it has a lower supersaturation and a larger buoyancy. This causes the polluted thermal to accelerate upward according to

$$\frac{d\hat{w}}{dt} = \hat{b} - \frac{3c_d}{8r}\hat{w}^2.$$

Recognizing that $\hat{w} = \Delta w + w$, $\hat{b} = \Delta b + b$, and $\frac{dw}{dt} = 0$, it follows that

$$\frac{d\Delta w}{dt} = \Delta b - \frac{3c_d}{8r}(2w\Delta w + \Delta w^2).$$

By expanding Δb with Eq. 4-13 and then dividing both sides of the equation by $\tilde{w}$, it can be shown that

$$\frac{d\Delta W}{dt} = \frac{\Delta b_0}{\tilde{w}} - \tau_b^{-1}\Delta W - \tau_{F_d}^{-1}\left(\Delta W + \frac{\Delta W^2}{2W}\right),$$

where $\Delta b_0 \equiv \frac{3aS}{8}(1-\beta)$, $\tau_b \equiv \frac{8w}{3aS\beta}$, and $\tau_{F_d} \equiv \frac{4r}{3c_d w}$. This equation predicts how warm-phase convective invigoration develops over time as the polluted thermal evolves towards its terminal velocity. The first term on the right side, $\Delta b_0/\tilde{w}$,

https://doi.org/10.5194/egusphere-2026-3985
Preprint. Discussion started: 24 July 2026

represents the initial buoyancy anomaly in the polluted thermal relative to the clean thermal. The second term is a restoring force from subsequent buoyancy changes in the polluted thermal. This term represents the fact that a faster updraft speed causes the supersaturation to rise, offsetting the initial buoyancy anomaly. The final term on the right side is a restoring force from changes in drag. This term represents the fact that a faster updraft speed strengthens the drag force, further offsetting the initial buoyancy anomaly. The coefficients τ_b and τ_{F_d} are the characteristic timescales for the restoring forces from buoyancy and drag, respectively.

The relative importance of the restoring forces is determined by their characteristic timescales. For instance, if the clean thermal rises slowly ($W \ll \left(\frac{\beta}{2}\right)^{1/2}$), then $\tau_b \ll \tau_{F_d}$. In this case the buoyancy of the polluted thermal adjusts rapidly after $t = 0$ s, but drag remains approximately constant (Fig. 4a). The invariance of drag requires that $\lim_{t\to\infty} \Delta b \approx 0$ m s^{-2}, which implies that $\lim_{t\to\infty} \Delta S \approx 0$. It follows from the quasi-steady relation for supersaturation that $\frac{\hat{w}}{w} \approx \frac{\hat{n}\hat{D}}{n\bar{D}} = \beta^{-1}$. This explains why the steady-state solution for ΔW is directly proportional to W when the clean thermal rises slowly (Eq. 16). A consequence is that warm-phase invigoration vanishes as $W \to 0$.

Warm-phase convective invigoration develops in a qualitatively different manner when the clean thermal rises rapidly ($W \gg \left(\frac{\beta}{2}\right)^{1/2}$). In this case $\tau_b \gg \tau_{F_d}$, so drag adjusts rapidly while buoyancy remains approximately constant (Fig. 4b). Because the drag force depends quadratically on the updraft speed, the change in drag that is needed to balance Δb_0 can be attained with a progressively smaller value of Δw as the updraft speed increases. This explains why warm-phase invigoration is negligible as $W \to \infty$.

Finally, the time-dependent solutions reveal the length scale over which the polluted thermal adjusts to its terminal velocity. If $W \gg \left(\frac{\beta}{2}\right)^{1/2}$, then the adjustment length scale is $w\tau_{F_d} = \frac{4r}{3c_d}$, which is approximately equal to the thermal diameter. If $W \ll \left(\frac{\beta}{2}\right)^{1/2}$, then the adjustment length scale is at least one order of magnitude smaller (Fig. 5). Thus, Δw attains at least 85% of its steady-state value after the polluted thermal has travelled a distance equal to only twice its diameter (for $c_d = 0.6$). The steady-state model is therefore justified for the purpose of predicting warm-phase invigoration.

https://doi.org/10.5194/egusphere-2026-3985
Preprint. Discussion started: 24 July 2026

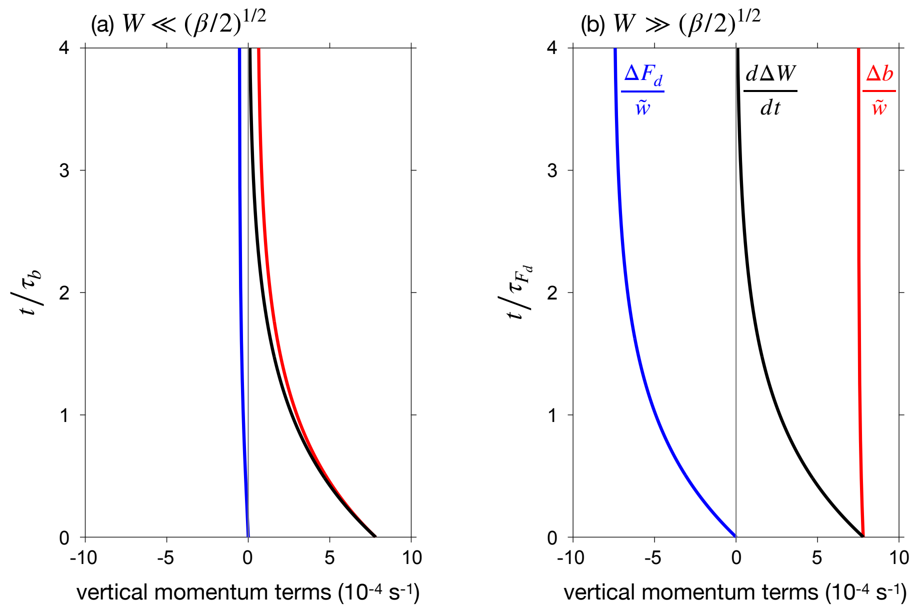

Figure 4: Vertical momentum budget for the time-dependent solutions. (a) Momentum terms for the case in which the clean thermal rises slowly ($W \ll \left(\frac{\beta}{2}\right)^{1/2}$). $\Delta F_d/\tilde{w}$, $d\Delta W/dt$, and $\Delta b/\tilde{w}$ are plotted as a function of t/τ_b, where τ_b is the buoyancy-adjustment timescale. (b) Similar to (a) but for the case in which the clean thermal rises rapidly ($W \gg \left(\frac{\beta}{2}\right)^{1/2}$). In this case, the time coordinate is t/τ_{F_d}, where τ_{F_d} is the drag-adjustment timescale. Values of $S = 1\%$ and $\frac{\hat{n}}{n} = 5$ are used. $W/\left(\frac{\beta}{2}\right)^{1/2}$ is set to 0.2 in (a) and 5 in (b). These values correspond to $w = 0.3$ m s^{-1} and $w = 6.5$ m s^{-1}, respectively.

https://doi.org/10.5194/egusphere-2026-3985
Preprint. Discussion started: 24 July 2026

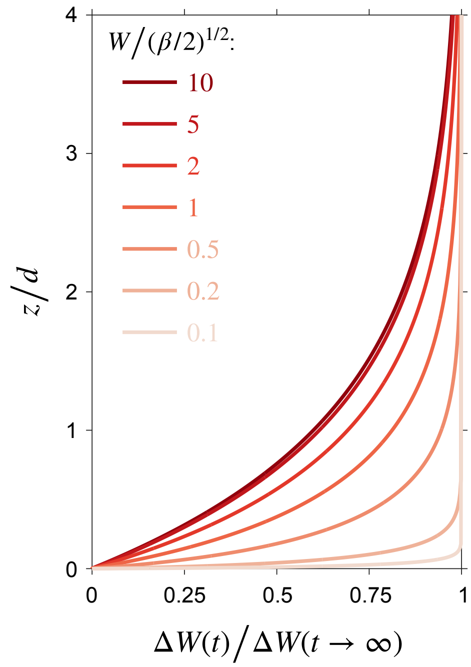

Figure 5: Adjustment length scale for time-dependent solutions. $\Delta W(t)/\Delta W(t\to\infty)$ is plotted as a function of z/d, where d is the diameter of the cloud thermal. Values of $S = 1\%$ and $\frac{\hat{n}}{n} = 5$ are used. $W/\left(\frac{\beta}{2}\right)^{1/2}$ is varied between 0.1 and 10. These values correspond to $w = 0.1$ m s^{-1} and $w = 13.1$ m s^{-1}, respectively.

3.3 Feedback Analysis

The way in which drag shapes warm-phase invigoration can be made more precise by framing the solutions in the language of formal feedback analysis. Consider a clean thermal initially in steady state. If the cloud-droplet number concentration suddenly changes from n to $\hat{n}$, then it creates a forcing that instantaneously reduces the supersaturation. This, in turn, increases the buoyancy and causes the thermal to accelerate upward. The upward acceleration strengthens the drag force, creating a negative feedback process. The thermal will continue to adjust until it reaches a new steady state. An analog could occur in natural clouds if cloud-condensation-nuclei activate episodically above the cloud base (Prabha et al., 2011).

In order to quantify how the feedback from changing drag shapes the steady-state response, a reference system without the feedback process must be established. I define the reference system as having a constant drag force. Warm-phase invigoration can then be expressed as

$$\Delta W = \frac{\Delta W_0}{1-f_d}.$$

https://doi.org/10.5194/egusphere-2026-3985
Preprint. Discussion started: 24 July 2026

where ΔW_0 is invigoration in the constant-drag reference system and f_d is the non-dimensional feedback factor that characterizes the feedback from changing drag. Expressions for ΔW_0 and f_d are derived following the framework of Roe (2009) in Appendix A.

ΔW_0 can be understood following similar logic to the time-dependent solutions in which the clean thermal rises slowly. Because the clean and polluted thermals experience the same drag force in the reference system, both thermals must have the same steady-state buoyancy and supersaturation. The relation for quasi-steady supersaturation in Eq. 11 implies that $\frac{\hat{w}}{w} = \frac{\hat{n}\hat{D}}{n\bar{D}} = \beta^{-1}$ is independent of w, and $\Delta W_0 = W\left(\frac{\hat{w}}{w} - 1\right) = W(\beta^{-1} - 1)$. This means that if the drag force were constant, then warm-phase invigoration would be strongest in clouds with the fastest updrafts (Fig. 6a).

f_d exhibits more interesting behavior. The general solution is a cumbersome function given by Eq. A3, but it can be simplified for the limiting cases in which the clean thermal rises slowly or rapidly:

$$f_d \approx \begin{cases} 0, \; W \ll \left(\frac{\beta}{2}\right)^{1/2} \\ 1 - \frac{2W^2}{\beta}, \; W \gg \left(\frac{\beta}{2}\right)^{1/2} \end{cases}.$$

Because drag is proportional to the updraft speed squared, f_d varies dramatically as a function of W (Fig. 6b). For example, if $W = 4$ and $\hat{n}/n = 5$, then $f_d \approx -100$. This feedback damps the response of the updraft speed by two orders of magnitude relative to the reference system (i.e. $(1 - f_d)^{-1} \approx 0.01$). In contrast, if $W \ll \left(\frac{\beta}{2}\right)^{1/2}$, then the drag feedback is weak enough that it can be ignored. The non-linear relationship between drag and updraft speed gives rise to a negative feedback that is negligible for slow updrafts but becomes increasingly powerful as updrafts rise faster.

Warm-phase invigoration in the full model depends on both ΔW_0 and f_d. If the clean thermal rises slowly, then the drag feedback provides very little resistance to convective invigoration, but ΔW_0 is also relatively small. If the clean thermal rises rapidly, then ΔW_0 is large, but the drag feedback strongly damps changes in the updraft speed. Warm-phase invigoration optimizes between these two limiting cases (Fig. 6c).

https://doi.org/10.5194/egusphere-2026-3985
Preprint. Discussion started: 24 July 2026

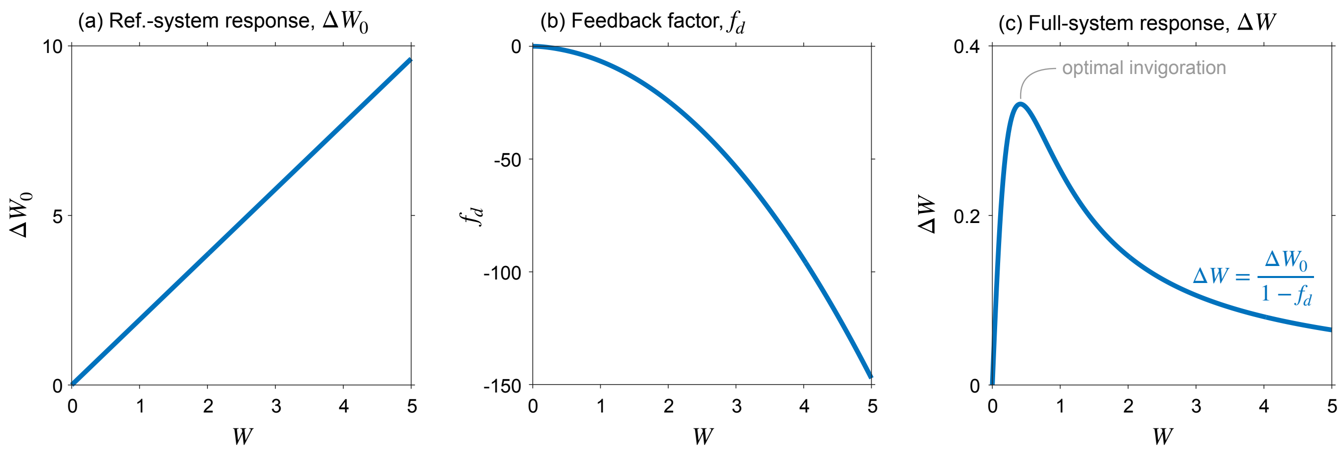

Figure 6: Feedback analysis for steady-state solutions. (a) Warm-phase invigoration in the reference system, in which the drag force is constant (ΔW_0). The solution is plotted in non-dimensional form. Values of $S = 1\%$ and $\frac{\hat{n}}{n} = 5$ are used. (b) Non-dimensional feedback factor that characterizes the negative feedback from variations in the drag force (f_d). (c) Warm-phase invigoration in the full system, in which the drag force is allowed to vary.

3.4 Upper Bounds and Necessary Conditions for Substantial Warm-Phase Invigoration

The optimal updraft speed for warm-phase invigoration, w^*, is found by identifying the maximum of Δw (Eq. 14). Solving for $d\Delta w/dw = 0$ leads to

$$w^* = \tilde{w}\left(\frac{\beta}{2}\right)^{1/2}. \tag{17}$$

The maximum amount of invigoration, Δw^*, is found by evaluating Δw with $w = w^*$:

$$\Delta w^* = \tilde{w}\left(\sqrt{1+\beta} - \sqrt{2\beta}\right).$$

Both w^* and Δw^* depend on the properties of the clean thermal (raS/c_d) and $\hat{n}/n$. The relative change in the optimal updraft speed is given by:

$$\frac{\Delta w^*}{w^*} = \sqrt{2 + 2\beta^{-1}} - 2.$$

This value depends only on $\hat{n}/n$.

The w^*vs. Δw^* phase space reveals the upper bound for warm-phase invigoration as a function of S and $\hat{n}/n$. If $S = 0.1\%$, then $\Delta w \leq 0.45$ m s^{-1} for all updraft speeds of the clean thermal and all changes in cloud-droplet number concentration up to a ten-fold increase (Fig. 7a). If $S = 1\%$ or $S = 10\%$, then the equivalent upper bounds are $\Delta w \leq 1.41$ m s^{-1} and $\Delta w \leq 4.46$ m s^{-1}, respectively. In a relative sense, the updraft speed increases between 27% and 136% under optimal conditions if $2 \leq \hat{n}/n \leq 10$ (Fig. 7b). This large relative change occurs when the clean updraft speed is ~0.4 m s^{-1} if $S = 0.1\%$, ~1.3 m s^{-1} if $S = 1\%$, and ~4.1 m s^{-1} if $S = 10\%$ (for $\frac{\hat{n}}{n} = 5$). In other words, warm-phase invigoration substantially

https://doi.org/10.5194/egusphere-2026-3985
Preprint. Discussion started: 24 July 2026

boosts updraft speeds in a relative sense under optimal conditions, but the updrafts that experience this boost may or may not be fast enough to be relevant for deep convection.

The analytical model can also predict the necessary conditions for substantial warm-phase invigoration. Let invigoration be defined as substantial if it increases the updraft speed by 25% or more in response to a five-fold increase in the cloud-droplet number concentration (i.e. $\frac{\hat{n}}{n} = 5$). The choice of $\frac{\hat{n}}{n} = 5$ represents the range of typical variability observed in the cloud-droplet number concentration, while the choice of a 25% threshold for the change in updraft speed is arbitrary (Boucher and Lohmann, 1995). By solving Eq. 14 for S, it can be shown that substantial warm-phase invigoration occurs if

$$S \geq S_{min} = \frac{(\Lambda^2+2\Lambda)w^2 c_d}{(1-\Lambda\beta-\beta)ra}$$

where S_{min} is the minimum supersaturation in the clean thermal that can support substantial invigoration and $\Lambda = 0.25$ is the minimum relative change in updraft speed that constitutes substantial invigoration. For an updraft speed of $w = 3$ m s^{-1} typical of shallow convective clouds, substantial invigoration occurs if $S \geq 0.9\%$ (Fig. 8). For a faster updraft speed of $w =$ 7 m s^{-1} typical of oceanic deep convection, substantial invigoration occurs if $S \geq 4.8\%$. For an even faster updraft speed of $w = 15$ m s^{-1} typical of continental deep convection, substantial invigoration occurs if $S \geq 22.1\%$. Shallow convective clouds thus require a much smaller supersaturation to experience substantial invigoration. This is a consequence of the fact that shallow convective updraft speeds are typically closer to w^* than deep convective updraft speeds (Fig. 7).

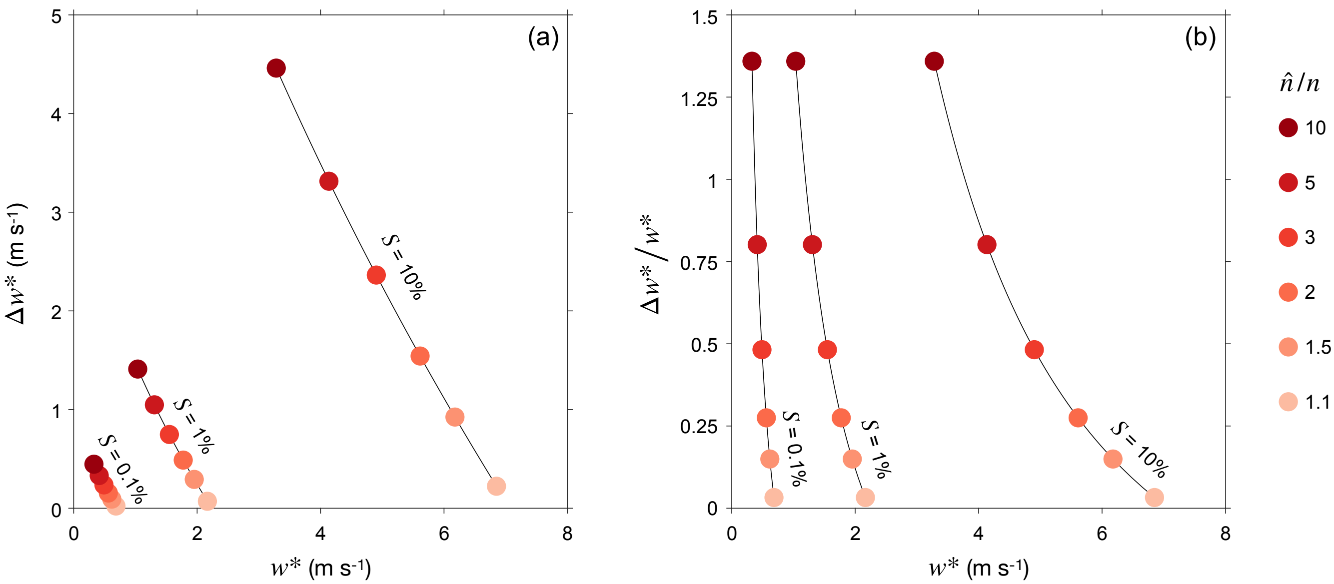

Figure 7: Optimal warm-phase invigoration. (a) Maximum warm-phase invigoration, Δw^*, plotted as a function of the updraft speed that experiences maximum invigoration, w^*. Solutions are plotted for $S = 0.1\%$, 1%, and 10% and for $\hat{n}/n$ ranging from 1.1 to 10, as indicated in the legend. Each point in this phase space corresponds to the peak of a curve representing Δw as a

https://doi.org/10.5194/egusphere-2026-3985
Preprint. Discussion started: 24 July 2026

function of w, such as those in Fig. 1. (b) Similar to (a), except that maximum warm-phase invigoration is plotted as a relative change rather than an absolute change.

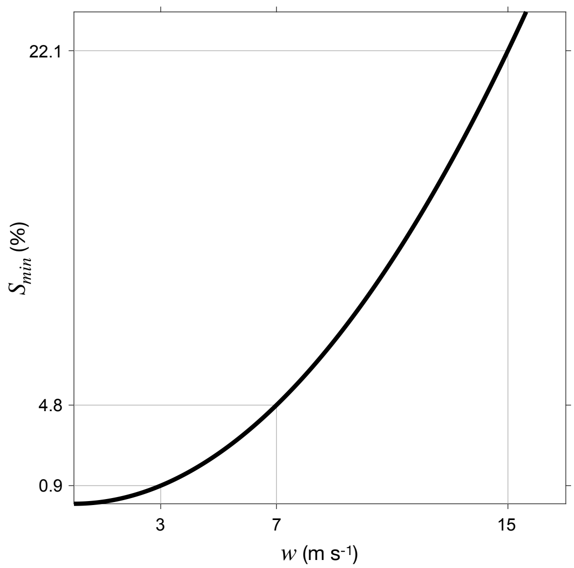

Figure 8: Necessary conditions for substantial warm-phase convective invigoration. Warm-phase invigoration is considered to be substantial if it causes the updraft speed to increase by 25% or more when the cloud-droplet number concentration increases by a factor of five. S_{min} is the minimum supersaturation in the clean thermal that can support substantial warm-phase invigoration.

3.5 Potential Observational Constraints

The theory developed here may provide opportunities for constraining estimates of warm-phase invigoration in nature. The solutions for Δw depend on several observable cloud properties (Eq. 14). Among these, S, c_d, and r are the most uncertain. S has been inferred from aircraft observations (Warner, 1968; Paluch and Knight, 1984; Politovich and Cooper, 1988; Prabha et al., 2011; Romps et al., 2023; Romps, 2025), and c_d and r have been inferred from stereophotogrammetry (Romps and Öktem, 2015). However, the sample size is quite small in both cases due to the difficulty of obtaining the necessary observations. New observational constraints on these properties could reduce uncertainty in warm-phase invigoration.

The potential for observational constraints is determined by varying S, c_d, and r across their ranges of plausible values. A reference case is defined with $S = 1\%$, $c_d = 0.6$, $r = 600$ m, $a = 1$ m s^{-2}, and $\hat{n}/n = 5$. The values of S, c_d, and r are then varied one at a time between 0.1% and 10%, 0.2 and 1, and 200 m and 1000 m, respectively. The spread in Δw from varying S is about three times larger than the spread in Δw from varying c_d and r (Fig. 9). Thus, observations that constrain supersaturation have the greatest potential to reduce uncertainty in cloud susceptibility to warm-phase invigoration.

https://doi.org/10.5194/egusphere-2026-3985
Preprint. Discussion started: 24 July 2026

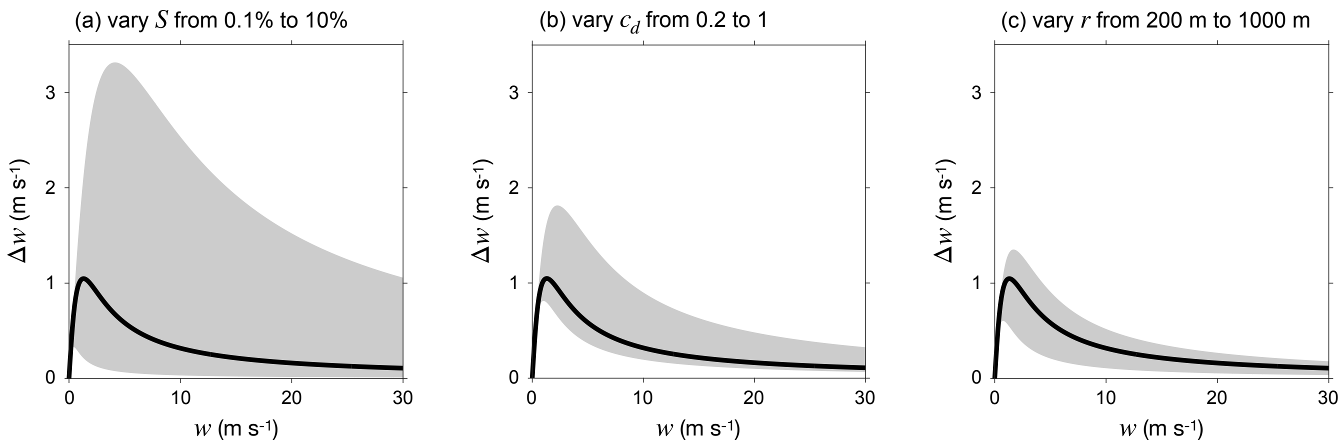

Figure 9: Potential observational constraints on warm-phase invigoration. (a) The black line shows a baseline solution for Δw as a function of w computed with $S = 1\%$, $c_d = 0.6$, $r = 600$ m, $a = 1$ m s^{-2} and $\hat{n}/n = 5$. Grey shading shows how the solutions change when S is varied from 0.1% to 10% with the other parameters fixed. (b) Similar to (a) except that S is set to the baseline value and c_d is varied from 0.2 to 1. (c) Similar to (a) except that S is set to the baseline value and r is varied from 200 m to 1000 m. These intervals span the range of plausible values for S, c_d, and r.

4 Key Assumptions

The analytical model makes several key assumptions that affect the accuracy of the solutions. One of these assumptions is that the radius and drag coefficient of the cloud thermals are prescribed to the midpoints of their typical ranges, including $r = 600$ m and $c_d = 0.6$. Individual deep convective clouds can deviate from these midpoint values. If $r = 1000$ m and $c_d = 0.2$, as suggested by some numerical simulations, then S_{min} is reduced by a factor of 5 (Hernandez-Deckers and Sherwood, 2016). Furthermore, thermals that take on a vertically elongated shape may experience weaker drag per unit mass than thermals that take on a spherical shape, as assumed in the theory. For this reason, the estimates of necessary conditions for substantial warm-phase invigoration in Fig. 8 may be too stringent for some deep convective situations.

Another key assumption is that the buoyancy difference between the cloud thermals can be approximated from temperature differences while neglecting water-vapor and hydrometeor-loading effects (Eq. 7). Let Δq be the difference in specific humidity between the two thermals at a particular height. Due to the conservation of moist static energy, Δq is associated with a temperature difference of $\Delta T = -L\Delta q/c_p$. Furthermore, by conservation of mass, Δq must also be associated with a change in the hydrometeor mixing ratio, Δq_H. This can be expressed as $\Delta q_H = -\Delta q(1-\eta)$, where η is the mass fraction of the hydrometeors that immediately falls out of the thermal as precipitation. Strictly speaking, the assumption that the two thermals have the same liquid water content implies that $\eta = 1$, but η is left unspecified here for a

https://doi.org/10.5194/egusphere-2026-3985
Preprint. Discussion started: 24 July 2026

more general estimate that applies even if liquid water content varies. A more accurate representation of buoyancy that includes water vapor and hydrometeor effects is given by

$$\Delta b \approx g\left(\frac{\Delta T}{T} + \left(\frac{R_v}{R_d} - 1\right)\Delta q - \Delta q_H\right) = g\Delta q\left(-\frac{L}{c_pT} + 1.61 - \eta\right),$$

where R_d is the specific gas constant for dry air and $\frac{L}{c_pT} \approx 9.1$ for $T = 273$ K. Neglecting water vapor and hydrometeor loading leads to an error in Δb of 7-21%. This constitutes a positive bias in Δb, so it causes the solutions to overestimate warm-phase invigoration.

The model also assumes that the two thermals have the same liquid water content in order to relate the mean droplet diameter to the droplet number concentration (Eq. 13). In other words, differences in the autoconversion and entrainment rates between the two thermals are ignored in this step. If the assumption of constant liquid water content is relaxed, then $LWC = LWC_a\kappa$ and $\widehat{LWC} = LWC_a\hat{\kappa}$, where LWC_a is the liquid water content in an adiabatic cloud parcel and κ and $\hat{\kappa}$ represent the ratio between the true liquid water content and the adiabatic liquid water content in the two thermals. It follows that $LWC = \widehat{LWC}\frac{\kappa}{\hat{\kappa}}$ and

$$\frac{\bar{D}}{\hat{\bar{D}}} = \left(\frac{n}{\hat{n}}\right)^{-1/3}\left(\frac{\kappa}{\hat{\kappa}}\right)^{1/3}.$$

By substituting this relation in place of Eq. 13, it can be shown that the solution for warm-phase invigoration is similar to Eq. 14 with β replaced by $\beta\left(\frac{\kappa}{\hat{\kappa}}\right)^{1/3}$. To bound $\kappa/\hat{\kappa}$, I note that an increase in cloud-droplet number concentration is expected to cause the precipitation rate to decrease or stay the same, implying that changes in autoconversion lead to $\frac{\kappa}{\hat{\kappa}} \leq 1$. A lower bound for $\kappa/\hat{\kappa}$ is expected when precipitating clouds are converted into non-precipitating clouds. According to satellite observations, this conversion is associated with $\frac{\kappa}{\hat{\kappa}} \geq 0.7$ (Lu et al., 2023). Thus, by allowing the autoconversion rate to change, w^* decreases by a factor of $\left(\frac{\kappa}{\hat{\kappa}}\right)^{1/6} \geq 0.94$. Changes in the entrainment rate are expected to cause errors of the same order of magnitude but opposite sign (Small et al., 2009). Thus, the use of constant liquid water content to infer $\bar{D}/\hat{\bar{D}}$ causes errors in optimal warm-phase invigoration of approximately 6% or less.

Another limitation is that the model does not explicitly consider vertical variations in the cloud-droplet number concentration. For this reason, the solutions are valid as long as the length scale of variation for n and $\hat{n}$ is much longer than the length scale of adjustment for ΔW when n and $\hat{n}$ are constant (L). This condition is equivalent to $\frac{dn}{dt} \ll \frac{n}{L/w}$ in a reference frame that follows the thermal. L is on the order of the thermal diameter (Fig. 5), w is on the order of 1 to 10 m s^{-1}, n is on the order of 10^1 to 10^3 cm^{-3}, and $\frac{dn}{dt}$ due to collision and coalescence is on the order of 10^{-5} to 10^{-2} cm^{-3} s^{-1} (Wood, 2006). Thus, the collision-coalescence process typically does not violate the conditions of validity for the model. Mechanisms that could temporarily violate the conditions of validity include secondary activation of cloud droplets above the cloud base or

https://doi.org/10.5194/egusphere-2026-3985
Preprint. Discussion started: 24 July 2026

sudden evaporation events from entrainment. Aside from these situations, the model is expected to accurately predict how warm-phase invigoration varies with height.

A final key assumption is that warm-phase invigoration can be predicted with environmental temperature held fixed. Tropical convective clouds interact with their environment to maintain negligible horizontal density gradients (Singh and O'Gorman, 2013). If a localized pollution plume perturbs some clouds inside a much larger area of non-polluted clouds, then the non-polluted clouds will constrain the environment, and the assumption of fixed environmental temperature is valid. However, if the pollution covers an area that is comparable to the entire convectively disturbed region of the tropics, then the environmental and cloud temperatures will change by approximately the same amount, and cloud buoyancy will remain constant (Seeley and Romps, 2016). This means that the analytical model can faithfully represent how convective clouds respond to localized aerosol anomalies, but it cannot predict how convective clouds respond to large-scale secular trends in aerosols. Some valid applications include warm-phase invigoration downstream of cities, volcanoes, shipping lanes, and other aerosol point sources.

5 Conclusion

This study develops an analytical model to predict warm-phase convective invigoration from aerosol-cloud interactions. The model extends a theory developed by Romps et al. (2023) by incorporating warm-cloud microphysics into the governing equations and presenting time-dependent solutions and formal feedback analysis to interpret the solutions. The main advantage of the model is that it predicts warm-phase invigoration as a function of several observable cloud properties, including supersaturation, the radius and drag coefficient for cloud thermals, and the fractional change in cloud-droplet number concentration between clean and polluted conditions. This framing facilitates opportunities to identify observational constraints for cloud susceptibility to warm-phase invigoration.

The model predicts that for any given perturbation in cloud-droplet number concentration, there exists an optimal updraft speed that experiences the largest warm-phase invigoration, w^* (Fig. 1). Updrafts that are much slower than w^* experience $\Delta w \propto w$ because their steady-state buoyancy is constrained to remain approximately constant as the cloud-droplet number concentration varies. A consequence is that warm-phase invigoration is negligible as $w \to 0$ m s^{-1}. Updrafts that are much faster than w^* are damped by a powerful negative feedback from changes in the drag force. Warm-phase invigoration maximizes in updrafts that have the same order of magnitude as w^*. The optimal updraft speed depends on supersaturation in the clean thermal and varies from approximately 0.4 m s^{-1} if $S = 0.1\%$ to approximately 4.1 m s^{-1} if $S = 10\%$ (for $\frac{\hat{n}}{n} = 5$) (Fig. 7).

An important next step is to determine how closely real clouds align with the conditions for optimal invigoration. Among the observable quantities in the analytical model, supersaturation offers the greatest opportunity for an observational constraint to answer this question (Fig. 9). Part 2 of this work calculates supersaturation from globally distributed aircraft

https://doi.org/10.5194/egusphere-2026-3985
Preprint. Discussion started: 24 July 2026

observations to constrain the predictions of the analytical model (Wall et al., 2026). This constitutes a global assessment of cloud susceptibility to warm-phase convective invigoration.

Appendix A: Feedback Analysis

The terms of the feedback analysis in Section 3.3 are derived from the framework of Roe (2009). The clean thermal exists in a steady state of b, w, F_d, S, and n. If the cloud-droplet number concentration is suddenly changed from n to $\hat{n}$, then it creates a forcing of the supersaturation, ΔS_f. This forcing instantaneously changes the supersaturation by an amount

$$\Delta S_f = F\frac{w}{\hat{n}\hat{\bar{D}}} - F\frac{w}{n\bar{D}} = S(\beta - 1)\ .$$

In response, the buoyancy, updraft speed, drag, and supersaturation all adjust until they reach a new steady state that is characterized by the properties of the polluted thermal, including $\hat{b}$, $\hat{w}$, $\widehat{F_d}$, and $\hat{S}$. The convective invigoration parameter, λ, is defined as the change in updraft speed per unit of supersaturation forcing: $\lambda \equiv \frac{\Delta w}{\Delta S_f}$.

In order to quantify how feedbacks shape the system response, a reference system without the relevant feedbacks must be defined. The reference system is defined such that the drag force is constant in order to highlight the feedback from changing drag. The drag law expressed in Eq. 6 is excluded from the equations of the reference system, and the drag force is instead expressed as a constant value. Because drag and buoyancy balance one another in steady state, constant drag implies that $\Delta b = 0$ m s^{-2} (Eq. 5). This, in turn, implies that the two thermals must have the same temperature and supersaturation in the reference system (Eq. 4, 7). It follows that

$$0 = \Delta S_f + \Delta S,$$

where ΔS is the change in supersaturation that is caused by Δw after the cloud-droplet number concentration changes from n to $\hat{n}$. This term is given by

$$\Delta S = F\frac{\hat{w}}{\hat{n}\hat{\bar{D}}} - F\frac{w}{\hat{n}\hat{\bar{D}}} = F\frac{w}{n\bar{D}}\left(\frac{1}{w}\right)\left(\frac{n\bar{D}}{\hat{n}\hat{\bar{D}}}\right)\Delta w = \frac{S\beta}{w}\Delta w.$$

The reference system convective invigoration parameter, λ_0, can be found from

$$\lambda_0 = \frac{\Delta w}{\Delta S_f} = -\frac{\Delta w}{\Delta S} = -\frac{w}{S\beta}.$$

Warm-phase convective invigoration in the reference system, Δw_0, is

$$\Delta w_0 = \lambda_0 \Delta S_f = w(\beta^{-1} - 1).$$

Normalizing by $\widetilde{w}$ leads to

$$\Delta W_0 = W(\beta^{-1} - 1). \quad \text{(A1)}$$

When the drag force is allowed to vary, it gives an additional nudge to the updraft speed, which then gives an additional nudge to the supersaturation. The nudge in supersaturation is represented as being proportional to the system response, $c_1\Delta w$, where c_1 is a constant. This representation is standard in formal feedback analysis, and it is consistent with

https://doi.org/10.5194/egusphere-2026-3985
Preprint. Discussion started: 24 July 2026

the supersaturation equation in the physical model (Roe, 2009; Eq. 11). By adding $c_1\Delta w$ to the supersaturation perturbation, the full-system response can be expressed as

$$\Delta w = \lambda_0(\Delta S_f + c_1\Delta w).$$

Solving for Δw and normalizing by $\tilde{w}$,

$$\Delta W = \frac{(\lambda_0\Delta S_f)/\tilde{w}}{1-c_1\lambda_0} = \frac{\Delta W_0}{1-f_d}, \quad \text{(A2)}$$

where $f_d \equiv c_1\lambda_0$ is the non-dimensional feedback factor. The inclusion of the drag feedback changes the response of the updraft speed by a factor of $(1-f_d)^{-1}$ relative to the reference system.

By solving Eq. A2 for f_d and then substituting the relationships for ΔW_0 and ΔW in Eq. A1 and Eq. 15, it can be shown that

$$f_d = 1 - \left(\frac{\beta-1}{\beta}\right)\left(1 + \frac{\beta}{2W^2} - \left(\left(\frac{\beta}{2W^2}\right)^2 + 1 + W^{-2}\right)^{\frac{1}{2}}\right)^{-1}. \quad \text{(A3)}$$

If $W \gg \left(\frac{\beta}{2}\right)^{1/2}$ or $W \ll \left(\frac{\beta}{2}\right)^{1/2}$, then f_d can be approximated with a second-order Taylor series expansion in $\left(W/\left(\frac{\beta}{2}\right)^{1/2}\right)^{-1}$ or $W/\left(\frac{\beta}{2}\right)^{1/2}$, respectively. The approximate solutions are given by

$$f_d \approx \begin{cases} 0, & W \ll \left(\frac{\beta}{2}\right)^{1/2} \\ 1 - \frac{2W^2}{\beta}, & W \gg \left(\frac{\beta}{2}\right)^{1/2}. \end{cases}$$

Code Availability

Matlab code to reproduce the figures in the manuscript is available from the corresponding author upon request.

Data Availability

All of the data in the manuscript is available via parameter values and formulas printed in the text.

Author Contributions

CJW: Conceptualization, formal analysis, funding acquisition, methodology, project administration, software, visualization, writing.

Competing Interests

The author declares that he has no conflict of interest.

Acknowledgements

I thank David Romps, Rusen Öktem, Adam Varble, Gunilla Svensson, Frida Bender, Guy Dagan, and Daniel Rosenfeld for helpful discussions. This work is funded by the European Union (ERC, AC3S, 101156240). Views and opinions expressed are however those of the author only and do not necessarily reflect those of the European Union or the European Research Council. Neither the European Union nor the granting authority can be held responsible for them.

References

Abbott, T. H., and Cronin, T. W.: Aerosol invigoration of atmospheric convection through increases in humidity. Science, *85*(January), 83–85. DOI: 10.1126/science.abc5181, 2021.

Bellouin, N., Quaas, J., Gryspeerdt, E., Kinne, S., Stier, P., Watson-Parris, D., Boucher, O., Carslaw, K. S., Christensen, M., Daniau, A. -L., Dufresne, J. -L., Feingold, G., Fiedler, S., Forster, P., Gettelman, A., Haywood, J. M., Lohmann, U., Malavelle, F., Mauritsen, T., McCoy, D. T., Myhre, G., Mülmenstädt, J., Neubauer, D., Possner, A., Rugenstein, M., Sato, Y., Schulz, M., Schwartz, S.E., Sourdeval, O., Storelvmo, T., Toll, V., Winker, D., and Stevens, B.: Bounding global aerosol radiative forcing of climate change. Rev. Geophys., 1–45. https://doi.org/10.1029/2019rg000660, 2020.

Boucher, O., and Lohmann, U.: The sulfate-CCN-cloud albedo effect. Tellus B: Chem. Phys. Meteorol., *47*(3), 281–300. https://doi.org/10.3402/tellusb.v47i3.16048, 1995.

Chua, X. R., and Ming, Y.: Convective Invigoration Traced to Warm-Rain Microphysics. Geophys. Res. Lett., *47*(23). https://doi.org/10.1029/2020GL089134, 2020.

Fan, J., Rosenfeld, D., Zhang, Y., Giangrande, S. E., Li, Z., Machado, L. A. T., Martin, S. T., Yang, Y., Wang, J., Artaxo, P., Barbosa, H. M. J., Braga, R. C., Comstock, J. M., Feng, Z., Gao, W., Gomes, H. B., Mei, F., Pöhlker, C., Pöhlker, M. L., Pöschl, U., and de Souza, R. A. F.: Substantial convection and precipitation enhancements by ultrafine aerosol particles. Science, *359*(6374), 411–418. https://doi.org/10.1126/science.aan8461, 2018.

Fan, J., Zhang, Y., Li, Z., Yan, H., Prabhakaran, T., Rosenfeld, D., and Khain, A.: Unveiling aerosol impacts on deep convective clouds: scientific concept, modeling, observational analysis, and future direction. J. Geophys. Res. Atmos., 1–22. https://doi.org/10.1029/2024JD041931, 2025.

Hernandez-Deckers, D., and Sherwood, S. C.: A Numerical Investigation of Cumulus Thermals. J. Atmos. Sci., 73, 4117–4136, https://doi.org/10.1175/JAS-D-15-0385.1, 2016.

Igel, A. L., and van den Heever, S. C.: Invigoration or Enervation of Convective Clouds by Aerosols? Geophys. Res. Lett., *48*(16), 1–10. https://doi.org/10.1029/2021GL093804, 2021.

Korolev, A. V., and Mazin, I. P.: Supersaturation of water vapor in clouds. J. Atmos. Sci., *60*(24), 2957–2974. https://doi.org/10.1175/1520-0469(2003)060<2957:SOWVIC>2.0.CO;2, 2003.

Lu, X., Mao, F., Rosenfeld, D., Zhu, Y., Zang, L., Pan, Z., and Gong, W.: The temperature control of cloud adiabatic fraction and coverage. Geophys. Res. Lett., 50, e2023GL105831. https://doi.org/10.1029/2023GL105831, 2023.

Morrison, H., and Peters, J. M.: Theoretical Expressions for the Ascent Rate of Moist Deep Convective Thermals. J. Atmos. Sci., 75(5), 1699-1719. https://doi.org/10.1175/JAS-D-17-0295.1, 2018.

Öktem, R., Romps, D. M., and Varble, A. C.: No Warm-Phase Invigoration of Convection Detected during GoAmazon. J. Atmos. Sci., 80, 2345–2364, https://doi.org/10.1175/JAS-D-22-0241.1, 2023.

Paluch, I. R., and Knight, C. A.: Mixing and evolution of cloud droplet size spectra in vigorous continental cumulus. J. Atmos. Sci., 41, 1801–1815. https://doi.org/10.1175/1520-0469(1984)041<1801:MATEOC>2.0.CO;2, 1984.

Politovich, M. K., and Cooper, W. A.: Variability of the supersaturation in cumulus clouds. J. Atmos. Sci., 45, 1651–1664. https://doi.org/10.1175/1520-0469(1988)045<1651:VOTSIC>2.0.CO;2, 1988.

Prabha, T. V., Khain, A., Maheshkumar, R. S., Pandithurai, G., Kulkarni, J. R., Konwar, M., and Goswami, B. N.: Microphysics of premonsoon and monsoon clouds as seen from in situ measurements during the Cloud Aerosol Interaction And Precipitation Enhancement Experiment (CAIPEEX). J. Atmos. Sci., *68*(9), 1882–1901. https://doi.org/10.1175/2011JAS3707.1, 2011.

Roe, G.: Feedbacks, Timescales, and Seeing Red. Annu. Rev. Earth Planet. Sci., *37*(1), 93–115. https://doi.org/10.1146/annurev.earth.061008.134734, 2009.

Romps, D. M.: A Method for Calculating Reliable Supersaturation Reveals Low Values in Tropical Rainy-Season Clouds. J. Atmos. Sci., *82*(8), 1517–1527. https://doi.org/10.1175/JAS-D-24-0265.1, 2025.

Romps, D. M., and Charn, A. B.: Sticky thermals: Evidence for a dominant balance between buoyancy and drag in cloud updrafts. J. Atmos. Sci., *72*(8), 2890–2901. https://doi.org/10.1175/JAS-D-15-0042.1, 2015.

Romps, D. M., and Öktem, R.: Stereo photogrammetry reveals substantial drag on cloud thermals. Geophys. Res. Lett., *42*(12), 5051–5057. https://doi.org/10.1002/2015GL064009, 2015.

Romps, D. M., Latimer, K., Zhu, Q., Jurkat-Witschas, T., Mahnke, C., Prabhakaran, T., Weigel, R., and Wendisch, M.: Air Pollution Unable to Intensify Storms via Warm-Phase Invigoration. Geophys. Res. Lett., *50*(2), 1–9. https://doi.org/10.1029/2022GL100409, 2023.

Rosenfeld, D., Lohmann, U., Raga, G. B., O'Dowd, C. D., Kulmala, M., Fuzzi, S., Reissell, A., and Andreae, M. O.: Flood or drought: How do aerosols affect precipitation? Science, *321*(5894), 1309–1313. https://doi.org/10.1126/science.1160606, 2008.

Seeley, J. T., and Romps, D. M.: Tropical cloud buoyancy is the same in a world with or without ice, Geophys. Res. Lett., 43, 3572–3579, doi:10.1002/2016GL068583, 2016.

Singh, M. S., and O'Gorman, P. A.: Influence of entrainment on the thermal stratification in simulations of radiative-convective equilibrium. Geophys. Res. Lett., *40*(16), 4398–4403. https://doi.org/10.1002/grl.50796, 2013.

Small, J. D., Chuang, P. Y., Feingold, G., and Jiang, H.: Can aerosol decrease cloud lifetime? Geophys. Res. Lett., *36*(16), 1–5. https://doi.org/10.1029/2009GL038888, 2009.

Thornton, J. A., Virts, K. S., Holzworth, R. H., and Mitchell, T. P.: Lightning enhancement over major oceanic shipping lanes. Geophys. Res. Lett., *44*(17), 9102–9111. https://doi.org/10.1002/2017GL074982, 2017.

https://doi.org/10.5194/egusphere-2026-3985
Preprint. Discussion started: 24 July 2026

Toll, V., Rahu, J., Keernik, H., Trofimov, H., Voormansik, T., Manshausen, P., Hung, E., Michelson, D., Christensen, M. W., Post, P., Junninen, H., Murray, B. J., Lohmann, U., Watson-Parris, D., Stier, P., Donaldson, N., Storelvmo, T., Kulmala, M., & Bellouin, N.: Glaciation of liquid clouds, snowfall, and reduced cloud cover at industrial aerosol hot spots. Science, *386*(6723), 756–762. https://doi.org/10.1126/science.adl0303, 2024.

Varble, A. C., Igel, A. L., Morrison, H., Grabowski, W. W., and Lebo, Z. J.: Opinion: A critical evaluation of the evidence for aerosol invigoration of deep convection. Atmos. Chem. Phys., *23*(21), 13791–13808. https://doi.org/10.5194/acp-23-13791-2023, 2023.

Wall, C. J., Varble, A. C., Öktem, R., and Romps, D. M.: A global assessment of warm-phase convective invigoration from aerosol-cloud interactions. Part 2: Observations. Atmos. Chem. Phys., 2026. (submitted concurrently with this manuscript)

Warner, J.: The supersaturation in natural clouds. J. Rech. Atmos., 3, 233–237, 1968.

Wood, R., Rate of loss of cloud droplets by coalescence in warm clouds, J. Geophys. Res., 111, D21205,doi:10.1029/2006JD007553, 2006.